

Hydrogen Sulfide Ligation in Hemoglobin I of *Lucina pectinata*—A QM/MM and Local Mode Study

Published as part of The Journal of Physical Chemistry A virtual special issue "Krishnan Raghavachari Festschrift".

Marek Freindorf, Juliana Antonio, and Elfi Kraka*



Cite This: *J. Phys. Chem. A* 2023, 127, 8316–8329



Read Online

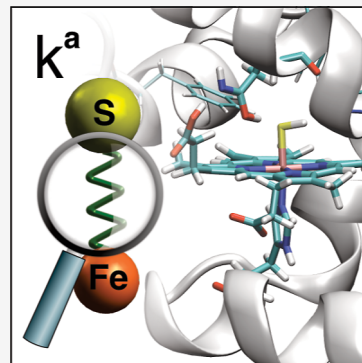
ACCESS |

Metrics & More

Article Recommendations

Supporting Information

ABSTRACT: In this study, we investigated the interaction between the H₂S ligand and the heme pocket of hemoglobin I (HbI) of *Lucina pectinata* for the wild-type protein; three known mutations where distal glutamine is replaced by hydrophobic valine (Gln64Val) and hydrophilic histidine in both protonation forms (Gln64His_e and Gln64His_d); five known mutations of the so-called phenyl cage, replacing the hydrophobic phenylalanines Phe29 and Phe43 with tyrosine (Tyr), valine (Val), or leucine (Leu); and two additional mutations, Phe68Tyr and Phe68Val, in order to complement previous studies with new insights about the binding mechanism at the molecular level. A particular focus was on the intrinsic strengths of the chemical bonds involved, utilizing local vibrational force constants based on combined quantum mechanical–molecular mechanical calculations. Wild-type protein and mutations clustered into two distinct groups: Group 1 protein systems with a proton acceptor in the distal protein pocket, close to one of the H₂S bonds, and Group 2 protein systems without a hydrogen acceptor close by in the active site of the protein. According to our results, the interactions between H₂S and HbI of *Lucina pectinata* involve two important elements, namely, binding of H₂S to Fe of the heme group, followed by the proton transfer from the HS bond to the distal residue. The distal residue is additionally stabilized by a second proton transfer from the distal residue to COO⁻ of the propionate group in heme. We could identify the FeS bond as a key player and discovered that the strength of this bond depends on two mutual factors, namely, the strength of the HS bond involved in the proton transfer and the electrostatic field of the protein pocket qualifying the FeS bond as a sensitive probe for monitoring changes in H₂S ligation upon protein mutations. We hope our study will inspire and guide future experimental studies, targeting new promising mutations such as Phe68Tyr, Phe68Val, or Phe43Tyr/Phe68Val.



INTRODUCTION

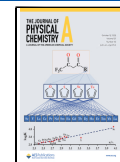
Hydrogen sulfide (H₂S) is a small gaseous molecule, which is produced in mammalian tissues. The precise physiological role of H₂S in biological systems is still largely unknown, although it may function as a gasotransmitter, neuromodulator, neuroprotector, and smooth muscle relaxant.^{1–9} Recently, the role of H₂S has been explored through the application of biomedicine, showing the diversity of this compound and the critical part it plays in a wide range of cellular events in physiological conditions.¹⁰ H₂S has also been suggested to be essential for many key necessities for the origin of life,^{9,11} serving as an important organic reactant, product, catalyst, and even a sustainable source of energy.^{12–14} Under physiological conditions, H₂S can easily dissociate into H⁺ and HS⁻, and both ligands (H₂S and HS⁻) can bind to the active site of hemeproteins.^{15–25} Hemeproteins are generally present in all organisms from bacteria to plants and animals.²⁶ Hemeproteins in vertebrate species, such as hemoglobin (Hb), myoglobin (Mb), or neuroglobin (Nb), are mainly responsible for O₂ binding in the ferrous Fe(II) oxidation state. Both Hb and Mb

can bind H₂S in the ferric Fe(III) state; however, the affinity is relatively low.¹⁸ Hemeproteins in nonvertebrate species can also bind H₂S, particularly for species living in sulfide-rich environments,²⁷ with the clam *Lucina pectinata* as one of the best studied nonvertebrate organisms.^{16,28} *Lucina pectinata* has a hemeprotein called hemoglobin I (HbI), which is responsible for delivering H₂S to the bacteria in order to maintain a symbiotic relationship. The affinity of H₂S for the ferric oxidation state of HbI is relatively high,¹⁷ and X-ray studies of HbI revealed that H₂S coordinated to the heme group in the protein active site, where histidine (His), which is typically present in the distal side of the heme pocket in hemeproteins, is replaced by glutamine (Gln).¹⁵ Moreover, in the active site

Received: June 29, 2023

Revised: August 31, 2023

Published: September 29, 2023



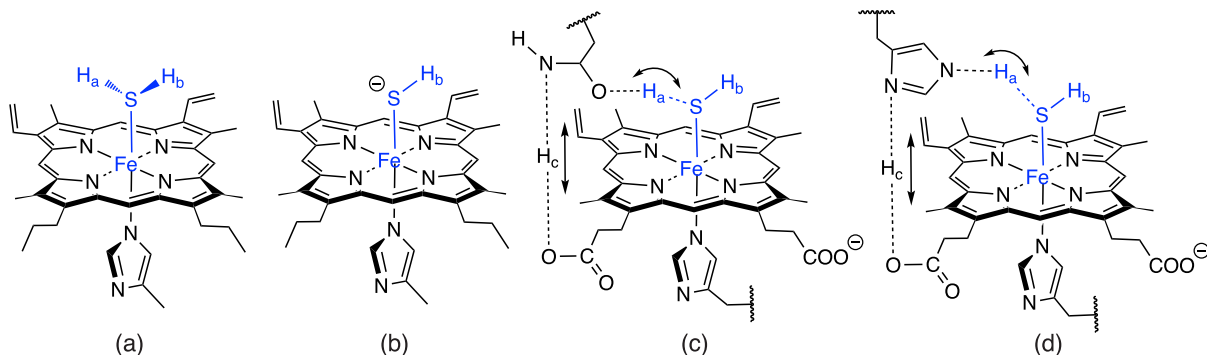


Figure 1. Schemes of selected molecular systems investigated in this study. (a) Gas-phase model of H_2S coordinated to the heme group (GasH₂S). (b) Gas-phase model of HS^- coordinated to the heme group (GasSH). (c) QM part of QM/MM calculations showing the product of double-proton transfer in the wild-type protein (WT). (d) QM part of QM/MM calculations showing the product of double-proton transfer in protein mutation (Gln64His). Selected hydrogen atoms are shown, and the bonds of special interest in this work are shown in blue color. For molecular labels, see the text.

of *Lucina pectinata*, there are three phenylalanines (Phe) oriented toward H_2S , which are generally known as the Phe cage.¹⁵

The properties of H_2S coordinated to HbI and the role of the surrounding amino acids and their mutations involving distal glutamine and Phe forming the Phe cage around H_2S in *Lucina pectinata* were investigated using experimental methods such as X-ray,¹⁵ resonance Raman measurements,¹⁷ UV-vis spectroscopy,¹⁶ and fluorescence spectroscopy.²⁹ The kinetics and dynamics of HbI ligand binding were experimentally investigated^{16,17,30} and complemented with theoretical studies utilizing hybrid molecular dynamics and combined quantum mechanical–molecular mechanical (QM/MM) calculations.^{17,21,24,31} Through these studies, they have found that the presence of distal Gln can be considered an adaptation to prevent loss of protein function for organisms living in a sulfide-rich environment, such as in the *Lucina pectinata*, and it has been argued that the distal Gln, along with the Phe cage, is critical for the stabilization and release of H_2S through hydrogen bonding, i.e., the strength of the hydrogen bond between the distal residue and the bound ligand regulates H_2S dissociation.^{17,31,32} Whereas these studies have led to important overall insights, a detailed analysis of the mechanism at the molecular level including the assessment of the intrinsic strength of these hydrogen bonds has been missing so far, as well as that of the FeS bond, which is also a key player in this process.

To fill this gap, we computationally investigated the wild-type protein and protein mutations where distal glutamine is replaced by hydrophobic valine (Gln64Val) and hydrophilic histidine in both protonation forms (Gln64His_ε and Gln64His_δ). We also explored the suggestion that once H_2S is inside the protein, the binding might be dictated by the free space in the distal site that is accessible (steric) or electrostatic constraints that are exerted by nearby residues,^{17,18,32} considering seven protein mutations of the Phe cage, replacing the hydrophobic Phe with hydrophilic tyrosine (Tyr) or by valine (Val), which has a smaller hydrophobic side chain. Mutations Phe29Tyr, Phe29Val, Phe29Leu, Phe43Tyr, and Phe43Val were observed experimentally,¹⁷ and Phe68Tyr and Phe68Val were added by us to explore the influence on the FeS bond. As a reference, we also included two gas-phase models of the active site involving the H_2S and HS^- ligands coordinated to the heme group as shown in Figure 1a,b.

Utilizing our vibrational mode analysis,^{33,34} complemented with Bader's quantum theory of atoms in molecule (QTAIM) analysis of the electron density $\rho(\mathbf{r})$ ^{35–37} and the natural bond orbital (NBO) analysis,³⁸ our study focused in particular on the following objectives:

1. To analyze the role of the FeS bond as an efficient probe for monitoring and assessing H_2S ligation in HbI
2. To quantify the strength of the SH_a bond (see Figure 1c,d) and its relation to the FeS bond and to the OH_a or NH_a bond
3. To investigate a potential second proton transfer between the distal residue and COO^- of the heme group and its influence on the HbI active site focusing on the NH_c bond (see Figure 1c,d)
4. To explore what happens in the case no proton acceptor is available for the interaction with the SH_a bond as found in mutations Gln64Val and Gln64His_ε.

As computational methodology, we used QM/MM. Originally developed by Warshel, Karplus, and Levitt,^{39,40} the QM/MM method has been subsequently applied in a wide range of complex molecular systems.^{41,42} Raghavachari was continuously extending the QM/MM method through a QM/QM approach, which combines two parts of a complex molecular system using two different levels of quantum mechanical theory.^{43–45} He also developed the molecules-in-molecules approach⁴⁶ based on the QM/QM method and applied it to a wide range of chemical processes.^{47–51} Although the QM/QM method better describes a mutual polarization and a charge transfer between different parts of proteins, for simplicity in this study, we use the original QM/MM method, where starting geometries are taken from X-ray experimental structure of the wild-type protein from *Lucina pectinata*.

■ COMPUTATIONAL DETAILS

As a qualified tool for assessing the intrinsic strength of a chemical bond or weak chemical interaction, we applied in this work local vibrational mode force constants k^a derived from the local vibrational mode analysis (LMA) developed in our group.^{33,34} LMA extracts specific information about the electronic structure and bonding of a molecule from the normal vibrational modes, which are produced during a routine frequency calculation.⁵² Normal vibrational modes are generally delocalized over a molecule,^{53–56} and therefore, associated normal mode frequencies and normal mode force

constants cannot serve as a direct measure of bond strength. The delocalization is caused by two types of normal mode coupling, kinematic and electronic couplings. The electronic coupling, which is reflected by the off-diagonal elements of the force constant matrix expressed in Cartesian coordinate x or internal coordinate q , is effectively removed during the frequency calculation via the Wilson GF formalism.⁵⁵ This involves transforming from Cartesian coordinates x to normal mode coordinates Q and related normal modes, resulting in a diagonal force constant matrix K^Q . However, this procedure does not eliminate the kinematic (mass) coupling reflected by the Wilson G (the so-called inverse kinetic energy matrix), which has often been overlooked. Konkoli and Cremer solved this problem by solving mass-decoupled Euler–Lagrange equations, in which the masses of all atoms of the molecule are set to zero except for those of the molecular fragment (such as bond, angle, or dihedral) undergoing the localized vibration of interest.^{57,58} By doing so, they were able to account for the effect of kinetic (mass) coupling and to derive for each molecular fragment being described by an internal coordinate q_n , the associated local vibrational mode a_n , local mode frequency ω^a , and force constant k^a .^{33,34,57,58} Local mode force constants k^a have proven to be a reliable tool to quantify the strength of covalent chemical bonds including metal–ligand bonds and weak chemical interactions, such as halogen, chalcogen, pnictogen, tetrel, or hydrogen bonding for molecules in gas phase, solution, and enzymes as well as for periodic systems, as summarized in refs 33 and 34 which also provide an in-depth description of the underlying theory of LMA.

For easier comparison, local mode force constants k^a can be transformed into relative bond strength orders (BSOs) via a power relationship of the form $BSO = A(k^a)^B$ according to the generalized Badger rule derived by Cremer, Kraka, and co-workers.^{59,60} The parameters A and B are obtained from two reference molecules with known BSO and k^a values and the request that a zero value of k^a corresponds to a BSO value of zero. The reference molecules used in our study are presented in Table 1. For bonds involving iron, we used Mayer's bond

Table 1. Bond Length R, Local Mode Force Constant k^a , and BSO of Selected Bonds in Reference Molecules Used in Our Study^a

bond	R (Å)	k^a (mDyn/Å)	BSO ^b	molecule
SH, NH	1.143	1.309	0.500	F_2H^-
	0.921	9.772	1.000	FH
FeH	1.543	1.977	0.889	FeH
	2.029	3.197	2.028	FeS

^aPBE/6-31G(d,p) level of theory. ^bBSO values of bonds involving Fe atom are based on Mayer's bond orders.^{61–63}

orders.^{61–63} The values of the power function parameters A and B for each bond discussed in this work are presented in the corresponding plots.

The LMA was complemented with Bader's QTAIM characterizing chemical bonds and weak chemical interactions based on topological features of the total electron density $\rho(\mathbf{r})$.^{35–37} In order to access the covalent character, we used the energy density H_ρ , which is a sum of the positive kinetic energy density G_ρ and the negative potential energy density V_ρ , taken at the bond critical point r_ρ between the two atoms forming the chemical bond/weak chemical interaction under consideration. According to the Cremer–Kraka criterion of

covalent bonding,^{64–66} a chemical bond/chemical interaction has predominantly covalent character when the potential energy density V_ρ dominates, accumulating the electron density at the bond critical point r_ρ leading to a negative value of H_ρ . If the value of H_ρ is positive, electrostatic interactions dominate.

Optimal geometries and vibrational frequencies of all HBIs investigated in this work were calculated with the hybrid Own N-layered Integrated molecular Orbital and Molecular mechanics (ONIOM), QM/MM method,⁶⁷ starting from the experimental X-ray structure of the wild-type HbI protein (Protein Data Bank (PDB) entry: 1MOH) of *Lucina pectinata* with H_2S ligated.¹⁵ Protein mutations were obtained using the Chimera program.⁶⁸ Hydrogen atoms were placed according to the standard Assisted Model Building with Energy Refinement (AMBER)⁶⁹ computational procedure, and the proteins were neutralized using six Na^+ counter-ions. The heme center was surrounded by a sphere of Transferable Intermolecular Potential with 3 Points (TIP3P)⁷⁰ water molecules, with a radius of 16 Å. The initial minimization with AMBER was followed by geometry optimization with ONIOM⁶⁷ using scaled electronic embedding. The QM part of the QM/MM calculations included the heme group with substituents, the side chains of proximal histidine, and the distal residue (glutamine or histidine), while the MM part included the rest of the protein system (see Figure 2). The QM/MM geometry optimizations were completed with QM/MM vibrational frequency calculations confirming no imaginary frequency values.

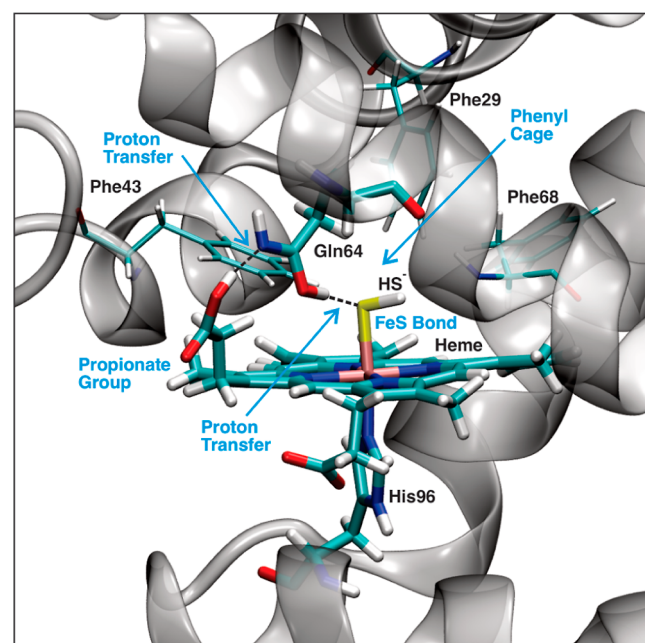


Figure 2. Illustration of the QM/MM description for wild-type HbI (WT).

Since the QM part of the investigated protein systems includes a transition metal, we used the PBE functional⁷¹ (which is a hybrid functional utilizing the 1998 revised version of the Perdew–Burke–Ernzerhof (PBE) pure functional⁷² for both the exchange and the correlation term), with the 6-31G(d,p) basis set⁷³ and the AMBER force field. PBE type functionals have proven to perform well for transition metal

Table 2. Properties of FeS Bond: Bond Length R , Local Mode Force Constant k^a , Energy Density at Bond Critical Point H_ρ , Fe Atomic Charge Q_{Fe} , S Atomic Charge Q_S , Charge Difference ΔQ , and BSO^a

FeS bond molecule	R Å	k^a mDyn/Å	H_ρ Hr/bohr ³	Q_{Fe} e	Q_S e	ΔQ e	BSO
WT	2.314	0.982	-0.0239	1.058	-0.510	1.568	0.268
Gln64Hie	2.487	0.308	-0.0102	1.131	-0.157	1.288	0.037
Gln64Hid	2.258	1.275	-0.0281	1.031	-0.520	1.551	0.419
Gln64Val	2.437	0.433	-0.0114	1.083	-0.086	1.169	0.066
Phe29Tyr	2.274	0.935	-0.0267	1.041	-0.515	1.556	0.246
Phe29Val	2.290	0.969	-0.0252	1.048	-0.523	1.570	0.262
Phe29Leu	2.286	0.908	-0.0256	1.046	-0.510	1.556	0.234
Phe43Tyr	2.230	1.087	-0.0237	1.057	-0.540	1.597	0.319
Phe43Val	2.281	0.969	-0.0262	1.045	-0.499	1.544	0.262
Phe68Tyr	2.289	0.966	-0.0252	1.047	-0.528	1.575	0.260
Phe68Val	2.293	1.111	-0.0250	1.049	-0.487	1.535	0.331
GasH2S	2.455	0.413	-0.0111	1.092	-0.108	1.199	0.061
GasSH	2.230	1.462	-0.0326	0.984	-0.409	1.392	0.530

^aFor molecular labels, see the text.

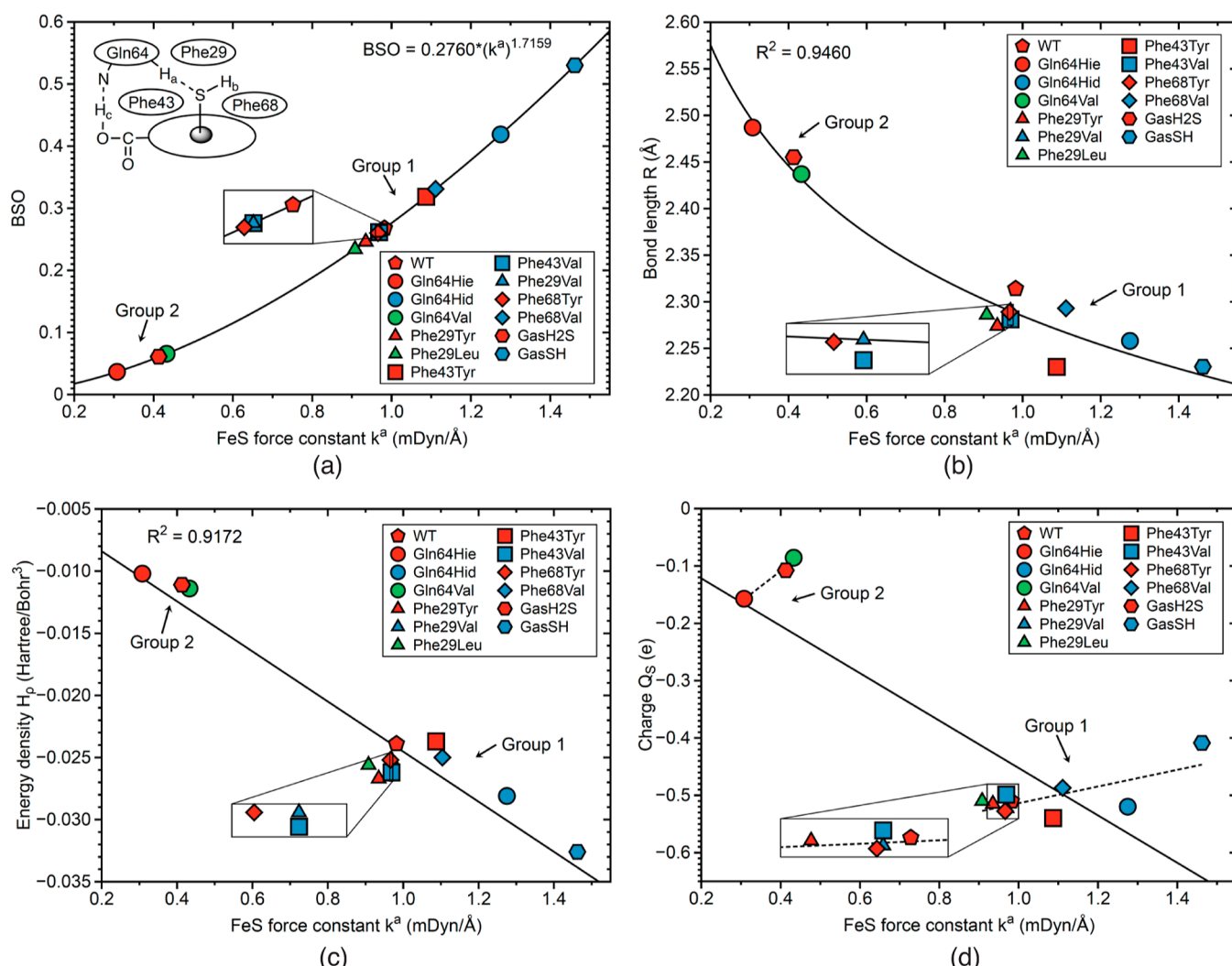


Figure 3. Properties of the FeS bond. (a) Relationship between local mode force constant k^a and BSO. (b) Correlation between local mode force constant k^a and bond length R . (c) Correlation between local mode force constant k^a and energy density H_ρ . (d) Relation between local mode force constant k^a and S atomic charge Q_S . For molecular labels, see the text.

complexes.^{74–77} The gas-phase calculations were done with a PBE0/6-31G(d,p) model chemistry. According to test QM/MM calculations, the PBE0 functional led to self-consistent

field (SCF) convergence for the molecular systems and correctly reproduced the FeN bond length in the gas-phase model of the ferric active site in bishistidyl hemeproteins. The

calculated FeN bond length of 1.965 Å in the ferric state turned out to be close to the experimental X-ray value of 1.970 Å for FeN in bis(1-methylimidazole) (*meso*-tetramesitylporphyrinato) Fe(III).⁷⁸ Geometry optimizations and frequency calculations were performed with Gaussian16,⁷⁹ and the LMA analysis was performed using the LModeA program.⁸⁰ The atomic charges were calculated with the NBO package,⁸¹ and the QTAIM analysis was performed using the AIMALL program.⁸² Images of the active site of all optimized geometries and the two gas-phase models are shown in the Supporting Information (Figures S2–S5).

RESULTS AND DISCUSSION

Starting from initial geometries with the neutral H₂S coordinated to the iron atom of the heme group for both wild type and all mutations, the QM/MM geometry optimizations led to two distinct groups: Group 1: WT, Gln64Hid, Phe29Tyr, Phe29Val, Phe29Leu, Phe43Tyr, Phe43Val, Phe68Tyr, Phe68Val, i.e., protein systems with an O or N atom close to the H_a atom of ligated H₂S and as such being able to form a hydrogen bond with H_a (see Figure 1c,d), and Group 2: Gln64Hie and Gln64Val, protein systems without a hydrogen acceptor close by in the active site of the protein. The optimized geometries of all Group 1 members confirm a proton transfer between the H_a atom of H₂S and the distal Gln64 or Gln64His_s residues, and in addition, a proton transfer between the distal NH_c atom and COO[−] of one propionate group of heme (see Figure 1c,d), i.e., a double-proton transfer mechanism. In contrast, for the Group 2 protein mutations, Gln64Hie and Gln64Val, the optimized geometries clearly reflect direct H₂S ligation to the iron center. It is interesting to note that the two gas-phase references GasSH (see Figure 1b) and GasH2S (see Figure 1a), cluster with Group 1 and Group 2 protein members, respectively. There is no direct correlation between R(SH_a) and R(SH_b) or between R(SH_a) and R(FeS), as depicted in Figure S1 of the Supporting Information; the clustering of protein systems into Groups 1 and 2 is obvious. In the following, a comprehensive characterization of the FeS, SH_a, and NH_c bonds is presented, amplifying the observations based on the optimized geometries.

FeS Bond. To our best knowledge, the FeS bond has not been a target of previous HbI studies. Inspired by our recent work on the assessment of Fe-ligand bonding in Mb⁸³ and in Nb⁸⁴ which led to a number of new mechanistic insights at the molecular level, we investigated in this work the intrinsic strength of the FeS bond and its role during the H₂S ligation process.

The molecular properties of the FeS bond inside wild-type HbI, along with 10 mutations studied in this work and the two gas-phase reference molecules, are presented in Table 2. Figure 3a shows the BSO values determined from k^a(FeS) via the power relationship based on the reference molecules presented in Table 1, Figure 3b presents the correlation between bond length R(FeS) and k^a(FeS), Figure 3c shows the correlation between the energy density H_p and k^a, and Figure 3d shows the correlation between the NBO charge on S and k^a.

The data in Table 2 and Figure 3 confirm that the FeS molecular properties cluster in two groups: Group 1 (WT, Gln64Hid, Phe29Tyr, Phe29Val, Phe29Leu, Phe43Tyr, Phe43Val, Phe68Tyr, Phe68Val, and GasSH) and Group 2 (Gln64Hie, Gln64Val, and GasH2S).

According to Table 2, the strongest FeS bond is found for the gas-phase reference with the HS[−] ligand (GasSH), as reflected by the largest local mode force constant value in this series ($k^a = 1.462 \text{ mDyn}/\text{\AA}$, BSO = 0.530), the shortest bond ($R = 2.230 \text{ \AA}$), and the most covalent character ($H_p = -0.0326 \text{ hartree}/\text{bohr}^3$). The second strongest FeS bond is found for the protein mutation where the distal glutamine is replaced by histidine in its δ protonation form (Gln64Hid with $k^a = 1.275 \text{ mDyn}/\text{\AA}$, $R = 2.258 \text{ \AA}$, and $H_p = -0.0281 \text{ hartree}/\text{bohr}^3$), whereas the FeS bond strength of the wild-type protein (WT) is in the medium range ($k^a = 0.982 \text{ mDyn}/\text{\AA}$, $R = 2.314 \text{ \AA}$, and $H_p = -0.0239 \text{ hartree}/\text{bohr}^3$). This shows that the FeS bond can serve as a sensitive probe to the protein environment, making it stronger for systems where the H_a atom can form a hydrogen bond between with the distal residue, which cannot happen in the gas-phase models or for Group 2 members. On the other end of the spectrum, the weakest FeS bond ($k^a = 0.308 \text{ mDyn}/\text{\AA}$) is found for the protein mutation where distal glutamine is replaced by histidine in its ϵ protonation form (Gln64Hie), which also has the longest bond ($R = 2.487 \text{ \AA}$) and the smallest covalent character ($H_p = -0.0102 \text{ hartree}/\text{bohr}^3$). The gas-phase model with H₂S (GasH2S) has the second weakest FeS bond (with $k^a = 0.413 \text{ mDyn}/\text{\AA}$, $R = 2.455 \text{ \AA}$, and $H_p = -0.0111 \text{ hartree}/\text{bohr}^3$), close to that of the protein mutation where distal glutamine is replaced by valine (Gln64Val; $k^a = 0.433 \text{ mDyn}/\text{\AA}$, $R = 2.437 \text{ \AA}$, and $H_p = -0.0114 \text{ hartree}/\text{bohr}^3$). These findings are illustrated in Figure 3a. The BSO values of Group 2 members as well as those for the gas-phase model GasH2S are small (ranging from 0.037 to 0.066), reflecting that ligation of H₂S leads only to a weak interaction of marginal covalent character. Even for Group 1 members, BSO values are relatively small compared to the Mayer's bond order of 0.889 for the FeH reference molecule (see Table 1), although their covalent character is increased compared to Group 2 members. These results support the experimental observation that H₂S transport and release are coupled in HbI to the ease of H₂S dissociation.^{10,17}

Figure 3b shows the correlation between $k^a(\text{FeS})$ and R(FeS), which largely follows the Badger rule^{60,85} ($R^2 = 0.9460$) that the shorter bond is also the stronger bond. An interesting exception from this rule is the Phe43Tyr protein mutation, which has the shortest bond of this series ($R = 2.230 \text{ \AA}$); however, it is not the strongest one ($k^a = 1.087 \text{ mDyn}/\text{\AA}$) and also not the most covalent one ($H_p = -0.0237 \text{ hartree}/\text{bohr}^3$). The exceptionally small FeS bond length in this protein mutation can be explained by the presence of an additional hydrogen bond, which is formed between the OH group from tyrosine and the S atom of the H₂S ligand being coordinated to the iron in the heme group. This leads to a bifurcated hydrogen bond between the S atom and two H atoms located in close proximity, forcing the S atom closer to the Fe atom, making the FeS bond shorter. As depicted by Figure 3c, there is a weak correlation ($R^2 = 0.9172$) between $k^a(\text{FeS})$ and H_p , again forming two clusters of FeS bonds, one including Group 1 members and another including Group 2 members, reflecting the different amount of covalent character of Group 1 and Group 2 members.

Figure 3d illustrates the relationship between $k^a(\text{FeS})$ and the S atomic charge Q_S . Q_S values for Group 1 members range between −0.55 and −0.40 e reflecting the shift of the H_a atom from the SH_a bond toward the O/N atom of the distal residue, whereas Q_S values of Group 2 members cover a considerably small range between −0.15 and −0.05 e. Within Group 1, we

Table 3. Properties of the SH_α Bond: Bond Length R , Local Mode Force Constant k^a , Energy Density at Bond Critical Point H_ρ , S Atomic Charge Q_S , H Atomic Charge Q_H , Charge Difference ΔQ , and BSO^a

SH_α bond molecule	R Å	k^a mDyn/Å	H_ρ Hr/bohr ³	Q_S e	Q_H e	ΔQ e	BSO
WT	2.253	0.189	-0.0023	-0.510	0.522	1.032	0.257
Gln64Hie	1.345	4.312	-0.1999	-0.157	0.206	0.363	0.754
Gln64Hid	2.313	0.141	-0.0004	-0.520	0.473	0.993	0.232
Gln64Val	1.345	4.303	-0.2006	-0.086	0.204	0.290	0.754
Phe29Tyr	2.199	0.207	-0.0026	-0.515	0.523	1.037	0.265
Phe29Val	2.202	0.177	-0.0024	-0.523	0.524	1.047	0.251
Phe29Leu	2.157	0.224	-0.0032	-0.510	0.518	1.027	0.272
Phe43Tyr	2.128	0.272	-0.0043	-0.540	0.511	1.051	0.291
Phe43Val	2.139	0.269	-0.0033	-0.499	0.519	1.018	0.290
Phe68Tyr	2.202	0.220	-0.0022	-0.528	0.526	1.054	0.270
Phe68Val	2.132	0.257	-0.0044	-0.487	0.508	0.995	0.285
GasH2S	1.346	4.298	-0.1994	-0.108	0.204	0.311	0.753

^aFor molecular labels, see the text.

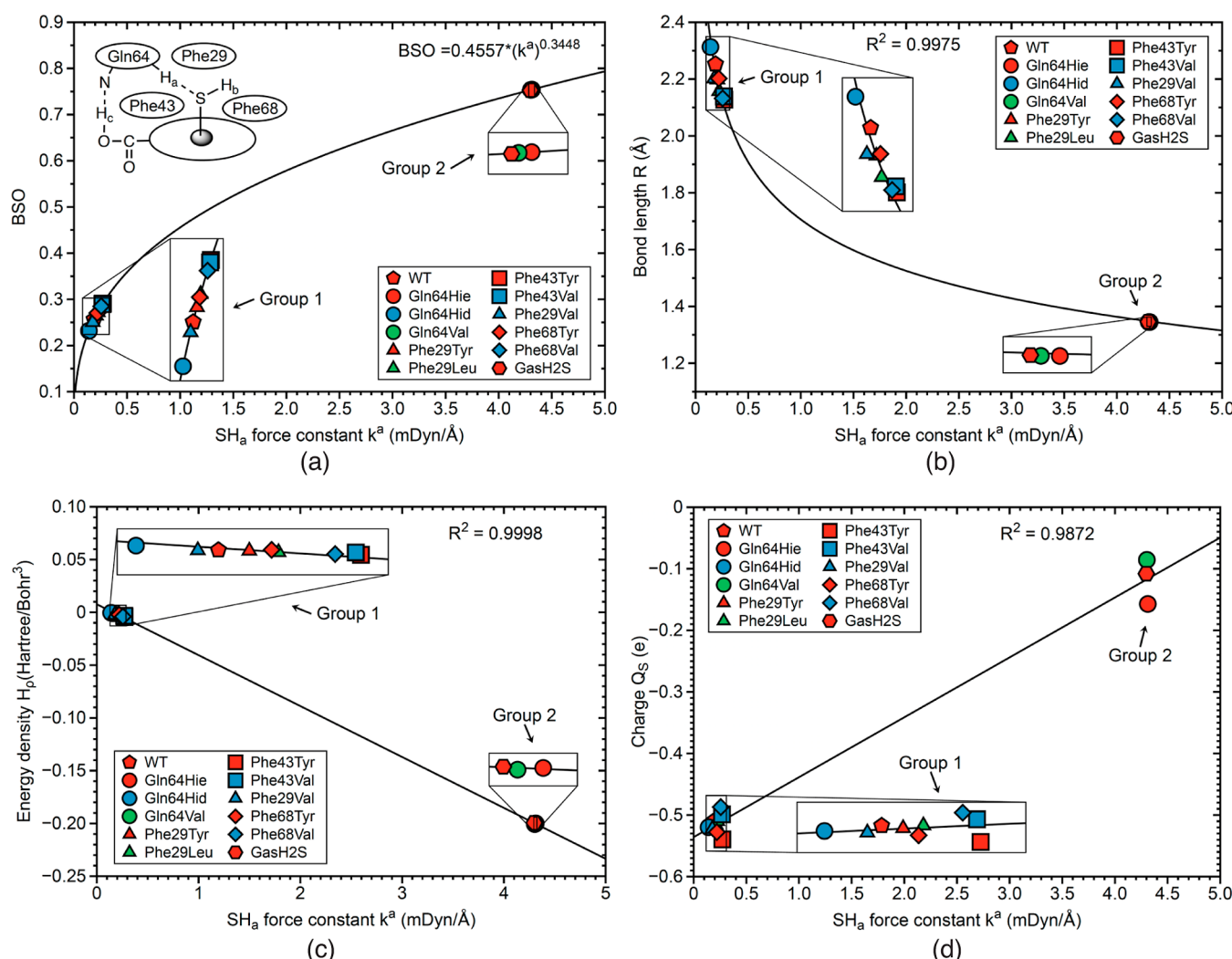


Figure 4. Properties of the SH_α bond. (a) Relationship between local mode force constant k^a and BSO. **(b)** Correlation between local mode force constant k^a and bond length R . **(c)** Correlation between local mode force constant k^a and energy density H_ρ . **(d)** Correlation between local mode force constant k^a and S atomic charge Q_S . For molecular labels, see the text.

observe that the S atoms become less negatively charged with increasing FeS bond strength, as denoted by the dashed line in Figure 3d. The Group 1 member with the strongest FeS bond (GasSH; $k^a = 1.462$ mDyn/Å) also has also the least negatively

charged S atom ($Q_S = -0.409$ e) found within this group, whereas the Group 1 member with the weakest FeS bond has a more negative S charge (Phe29Leu; $k^a = 0.908$ mDyn/Å, $Q_S = -0.510$ e). Phe43Tyr has the most negatively charged S atom

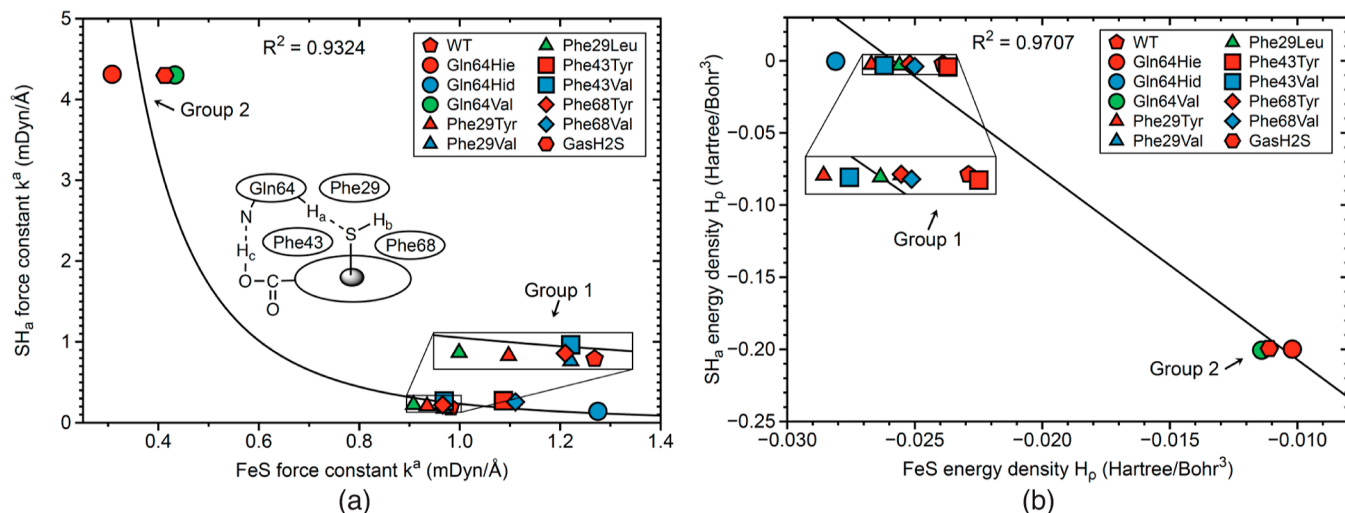


Figure 5. (a) Correlation between FeS force constant and SH_a force constant. (b) Correlation between FeS energy density and SH_a energy density. For molecular labels, see the text.

(Q_S of -0.540 e), although the corresponding FeS bond is not the weakest in this group ($k^a = 1.087$ mDyn/Å). This exception results from bifurcated hydrogen bonding taking place in **Phe43Tyr**. A similar trend between k^a (FeS) and the S atomic charge Q_S holds also for Group 2 members, as denoted by the dashed line in Figure 3d. The strongest FeS bond of Group 2 is found for **Gln64Val** ($k^a = 0.433$ mDyn/Å), which has also the least negatively charged S atom ($Q_S = -0.086$ e).

There are two effects that influence the S atomic charge: (i) the strength of the OH_a or NH_a hydrogen bond formed between the H_a atom and the distal residue, which is only present in Group 1, and (ii) the electrostatic potential of the heme pocket, which polarizes the S–H or S–Fe bond and which affects the members of both groups. Although the FeS bond in **GasSH** is the strongest overall, Group 1 members with weaker FeS bonds have more negatively charged S atoms, which indicates that the FeS bond strength is influenced to a large degree by the protein environment and that k^a (FeS) is a sensitive probe for this effect. In the **Gln64Hid** protein mutation, distal glutamine is replaced by histidine, which leads to a stronger interaction with the H_a atom and as such increasing the negative charge on the S atom ($Q_S = -0.520$ e). In the **Phe43Tyr** protein mutation, the formation of a bifurcated hydrogen bonding situation leads to the most negatively charged S atom in this series ($Q_S = -0.540$ e), although the strength of the corresponding FeS bond is in the medium range ($k^a = 1.087$ mDyn/Å), again qualifying k^a (FeS) as an efficient probe monitoring HbI H₂S ligation at the molecular level.

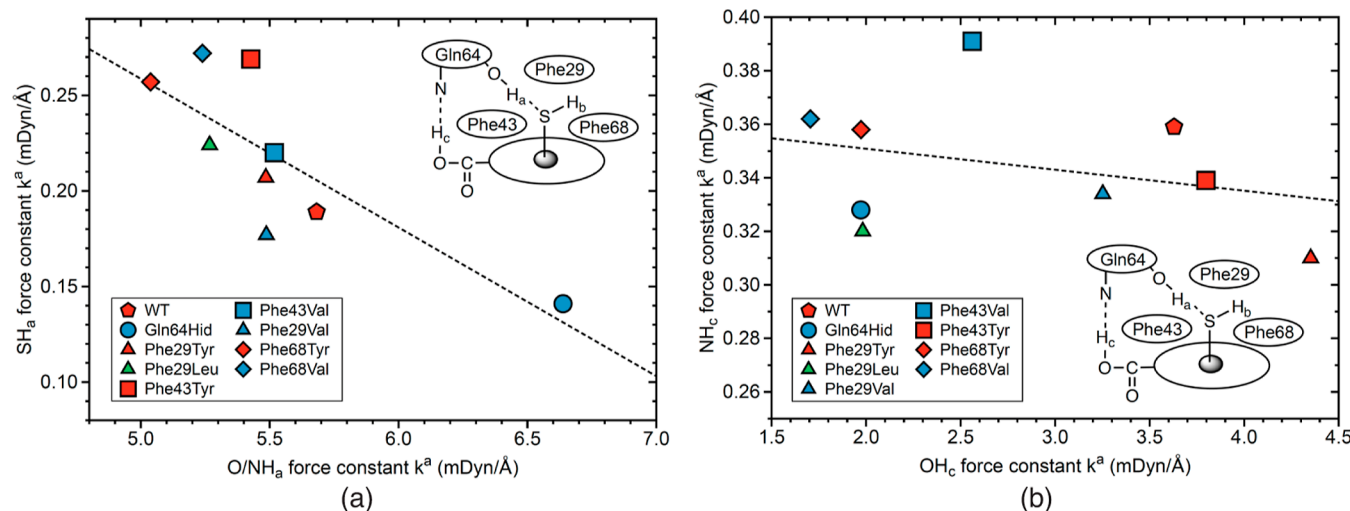
SH_a Bond. Although it has been experimentally suggested that the hydrogen bonding that occurs at the distal heme pocket for the OH_a bond or the NH_a bond plays a key role for the H₂S ligation process, our study explored if the SH_a bond can serve for the same purpose. The properties of the SH_a chemical bond, which involves the transferring of a proton, for H₂S coordinated to Fe of the heme group for the molecular systems investigated in our study are presented in Table 3. The relations between the selected properties of this bond are graphically represented in plots of Figure 4. Similar to the FeS bond, there are two groups (Groups 1 and 2) of molecular systems involving the SH_a bond. Figure 4a shows the relationship between the local mode force constant of the FeS bond and the SH_a bond revealing an interesting discovery, which additionally supports the use of the FeS bond as a probe for studying H₂S ligation. As mentioned previously, the stronger FeS bond correlates with a weaker SH_a bond, and the stronger FeS bonds are from the Group 1 proteins, where the double-proton transfer occurs, thus weakening the SH_a bond as it is the hydrogen bond donor, transferring the H_a atom to the O or N atom of the distal residues, serving as hydrogen bond acceptors, and forming the O/NH_a bond as depicted in Figure 1c,d. As obvious from Figure 5a, there is a general trend that a stronger FeS bond correlates with a weaker SH_a bond in this group. The same holds for the covalency, as shown in Figure 5b. The strongest FeS bond **Gln64Hid** ($k^a = 1.275$ mDyn/Å) corresponds to the weakest SH_a bond for this molecular

SH_a bond and its BSO. According to Table 3, the strongest SH_a bond that is observed in our calculations is in **Gln64Hie** ($k^a = 4.312$ mDyn/Å) for the systems in Group 2, and the weakest SH_a bond is in **Gln64Hid** ($k^a = 0.141$ mDyn/Å) in Group 1. In Figure 4b, we also indicate, with relatively good correlation ($R^2 = 0.9975$), that a stronger SH_a bond is correlated with a corresponding shorter bond. The SH_a average bond length in Group 2 is in the range of 1.35 Å, while for Group 1, the SH_a average bond length is in the range of 2.20 Å, clearly indicating a proton transfer process for Group 1, whereas in Group 2, no proton transfer process occurs. The correlation between the SH_a force constant and energy density at the bond critical point is shown in Figure 4c. According to Figure 4c, the molecular systems of Group 2 have a relatively large covalent character, which is confirmed by a much more negative value of the average energy density ($H_p = -0.2000$ hartree/bohr³) than in the molecular systems of Group 1 ($H_p = -0.0028$ hartree/bohr³). Figure 4d shows a relation between SH_a force constant and S atomic charge, indicating that a stronger SH_a bond correlates with a less negative S charge, while a weaker SH_a bond corresponds to a more negative charge on this atom. Overall, the properties investigated for this SH_a bond show that after the proton transfer from H₂S to O/N for Group 1 proteins, there is a weakening of the SH_a bond, coupled with a decrease in covalency and an increase in negative charge on S.

Figure 5a shows the correlation between the local mode force constant of the FeS bond and the SH_a bond revealing an interesting discovery, which additionally supports the use of the FeS bond as a probe for studying H₂S ligation. As mentioned previously, the stronger FeS bond correlates with a weaker SH_a bond, and the stronger FeS bonds are from the Group 1 proteins, where the double-proton transfer occurs, thus weakening the SH_a bond as it is the hydrogen bond donor, transferring the H_a atom to the O or N atom of the distal residues, serving as hydrogen bond acceptors, and forming the O/NH_a bond as depicted in Figure 1c,d. As obvious from Figure 5a, there is a general trend that a stronger FeS bond correlates with a weaker SH_a bond in this group. The same holds for the covalency, as shown in Figure 5b. The strongest FeS bond **Gln64Hid** ($k^a = 1.275$ mDyn/Å) corresponds to the weakest SH_a bond for this molecular

Table 4. Properties of OH_a and NH_a Bonds: Bond Length R, Local Mode Force Constant k^a, Energy Density at Bond Critical Point H_ρ, O/N Atomic Charge Q_{ON}, H Atomic Charge Q_H, Charge Difference ΔQ, and BSO^a

O/NH _a molecule	bond	R Å	k ^a mDyn/Å	H _ρ Hr/bohr ³	Q _{ON} e	Q _H e	ΔQ e	BSO
WT	OH _a	0.993	5.682	-0.5466	-0.744	0.522	1.265	0.829
Gln64Hid	NH _a	1.017	6.638	-0.5055	-0.538	0.473	1.011	0.875
Phe29Tyr	OH _a	0.994	5.485	-0.5458	-0.732	0.523	1.254	0.819
Phe29Val	OH _a	0.992	5.487	-0.5522	-0.739	0.524	1.263	0.820
Phe29Leu	OH _a	0.995	5.267	-0.5447	-0.734	0.518	1.251	0.808
Phe43Tyr	OH _a	0.999	5.239	-0.5303	-0.742	0.511	1.253	0.807
Phe43Val	OH _a	0.993	5.427	-0.5473	-0.726	0.519	1.245	0.816
Phe68Tyr	OH _a	0.992	5.518	-0.5526	-0.732	0.526	1.258	0.821
Phe68Val	OH _a	1.002	5.038	-0.5216	-0.748	0.506	1.254	0.796

^aFor molecular labels, see the text.**Figure 6. Relations between hydrogen bond properties. (a) Relation between local mode force constants k^a of OH_a (NH_a bond for Gln64Hid) and SH_a bonds. (b) Relation between local mode force constants k^a of the OH_c and NH_c bonds. For molecular labels, see the text.****Table 5. Properties of the SH_b Bond: Bond Length R, Local Mode Force Constant k^a, Energy Density at Bond Critical Point H_ρ, S Atomic Charge Q_S, H Atomic Charge Q_H, Charge Difference ΔQ, and BSO^a**

SH _b bond molecule	R Å	k ^a mDyn/Å	H _ρ Hr/bohr ³	Q _S e	Q _H e	ΔQ e	BSO
WT	1.347	4.228	-0.1957	-0.510	0.163	0.673	0.749
Gln64Hie	1.347	4.249	-0.1992	-0.157	0.214	0.371	0.750
Gln64Hid	1.345	4.265	-0.1977	-0.520	0.170	0.690	0.751
Gln64Val	1.347	4.241	-0.1996	-0.086	0.199	0.285	0.750
Phe29Tyr	1.347	4.238	-0.1942	-0.515	0.194	0.709	0.750
Phe29Val	1.345	4.265	-0.1959	-0.523	0.176	0.699	0.751
Phe29Leu	1.345	4.267	-0.1962	-0.510	0.174	0.684	0.751
Phe43Tyr	1.346	4.259	-0.1958	-0.540	0.178	0.717	0.751
Phe43Val	1.346	4.254	-0.1961	-0.499	0.170	0.668	0.751
Phe68Tyr	1.345	4.267	-0.1963	-0.528	0.172	0.699	0.751
Phe68Val	1.347	4.223	-0.1960	-0.487	0.165	0.652	0.749
GasH2S	1.346	4.308	-0.1998	-0.108	0.205	0.312	0.754

^aFor molecular labels, see the text.

system ($k^a = 0.141$ mDyn/Å), and the weakest FeS bond Phe29Leu ($k^a = 0.908$ mDyn/Å) corresponds to a relatively strong SH_a bond for this molecular system in this group ($k^a = 0.224$ mDyn/Å). On the contrary, in the molecular systems of Group 2, the average FeS local mode force constant ($k^a = 0.385$ mDyn/Å) is much smaller than the average SH_a force constant in this group ($k^a = 4.304$ mDyn/Å). Figure 5b shows

a similar correlation between the energy density at the bond critical point of the FeS bond and the SH_a bond. The average energy density of the FeS bond in the molecular systems of Group 1 ($H_\rho = -0.026$ hartree/bohr³) is more negative than the average energy density of the SH_a bond in this group ($H_\rho = -0.003$ hartree/bohr³), indicating a much covalent character of the FeS bond in this group. In contrast, in protein mutations in

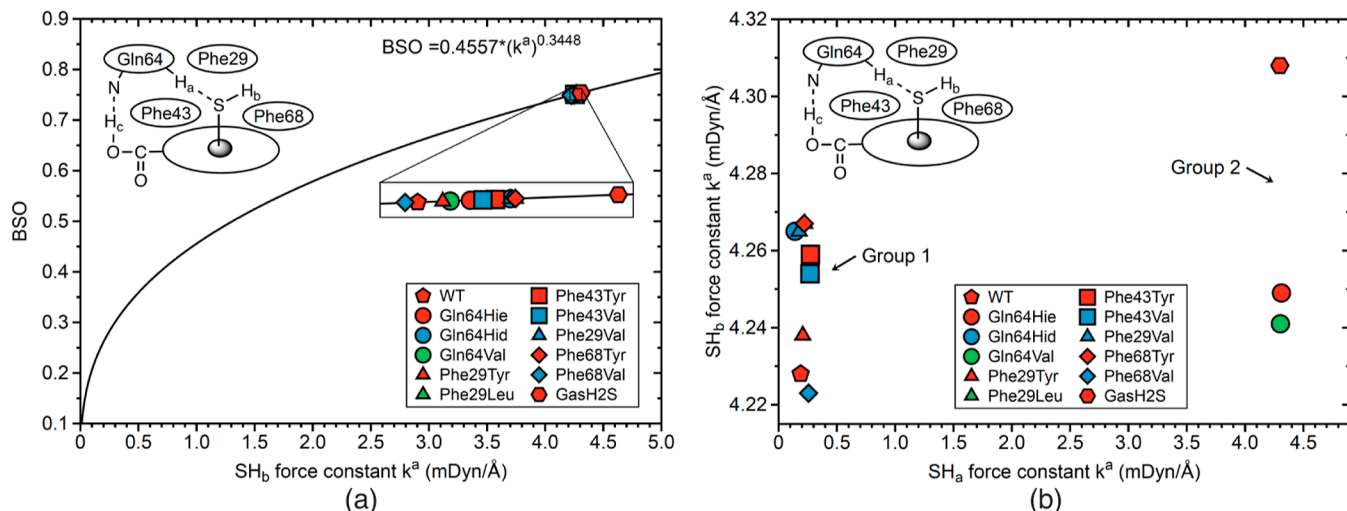


Figure 7. Properties of the SH_b bond. (a) Relationship between local mode force constant k^a of SH_b bond and BSO. (b) Correlation between local mode force constants k^a of SH_a and SH_b bonds. For molecular labels, see the text.

Table 6. Properties of the NH_c Bond: Bond Length R, Local Mode Force Constant k^a , Energy Density at Bond Critical Point H_ρ , N Atomic Charge Q_N , H Atomic Charge Q_H , Charge Difference ΔQ , and BSO^a

NH_c bond molecule	R Å	k^a mDyn/Å	H_ρ Hr/bohr ³	Q_N e	Q_H e	ΔQ e	BSO
WT	1.628	0.359	-0.0110	-0.855	0.515	1.370	0.320
Gln64Hid	1.515	0.328	-0.0316	-0.591	0.521	1.111	0.310
Phe29Tyr	1.692	0.310	-0.0059	-0.862	0.518	1.380	0.304
Phe29Val	1.613	0.334	-0.0127	-0.840	0.516	1.355	0.312
Phe29Leu	1.517	0.320	-0.0295	-0.810	0.513	1.323	0.308
Phe43Tyr	1.481	0.362	-0.0400	-0.817	0.508	1.326	0.321
Phe43Val	1.642	0.339	-0.0096	-0.862	0.519	1.381	0.314
Phe68Tyr	1.547	0.391	-0.0231	-0.823	0.513	1.336	0.330
Phe68Val	1.520	0.358	-0.0295	-0.820	0.511	1.331	0.320

^aFor molecular labels, see the text.

which no proton transfer is able to occur (Group 2), the SH_a bond has a more covalent (the average $H_\rho = -0.200$ hartree/bohr³) and stronger bond character, while the FeS bond is weakened and becomes significantly much less covalent (the average $H_\rho = -0.011$ hartree/bohr³).

We also investigated in our study the hydrogen acceptor O/ NH_a bonds, which has been suggested in the literature as a key player for the HbI H_2S ligation^{17,31,32} with an emphasis on their relation to the SH_a bond. As revealed by the data in Table 4, the O and N hydrogen acceptor atoms of the distal residues form strong O/ NH_a bonds with BSO values in the range 0.796–0.829, with typical OH or NH bond lengths. However, the properties Gln64Hid with a NH_a bond differ considerably from the OH_a bond properties, as illustrated in Figure S2 of the Supporting Information.

Figure 6a shows the relationship between k^a of the hydrogen acceptor bond O/ NH_a and k^a of the hydrogen atom donor bond SH_a , while Figure 6b presents the relation between OH_c and NH_c force constants. There is the trend that stronger O/ NH_a bonds are connected with weaker SH_a bonds and vice versa, further confirming that the protein environments can be measured through the FeS bond as a probe and that the SH_a bond is a good representation of the O/ NH_a bonds.

We also investigated the SH_b spectator bond (see Figure 1c,d) which is not involved in the H_2S ligation process. As confirmed by the data in Table 5, bond lengths and molecular

properties of all protein SH_b bonds investigated in this work are quite similar and there is no difference with regard to the gas-phase reference model GasH2S, i.e., there is no influence of the protein environment, confirming their spectator bond status.

The BSO values of all SH_b bonds cluster around one value, as shown in Figure 7a confirming the data in Table 5. As depicted in Figure 7b, there is no obvious correlation between $k^a(\text{SH}_a)$ and $k^a(\text{SH}_b)$ values; however, it is interesting to note that the data points cluster into Group 1 and Group 2 members.

NH_c Bond. According to previous findings,^{17,31,32} the proton transfer between H_2S coordinated to the heme group and the distal residue (Gln64 and His64δ) stabilizes the protein active site. However, as already indicated by the optimized geometries discussed above, this proton transfer is accompanied by another proton transfer that occurs between the distal residue and COO⁻ of one propionate heme group involving the NH_c bond (see Figures 1c,d and S2–S4 in Supporting Information), which additionally stabilizes the protein active site. In the following, we discuss how this is reflected by the properties of the NH_c bond which are presented in Table 6 and visualized in Figure 8.

According to Figure 8a–c, the strongest NH_c bond is observed for Phe68Tyr ($k^a = 0.391$ mDyn/Å), which is not the shortest bond ($R = 1.547$ Å) and not the most covalent ($H_\rho =$

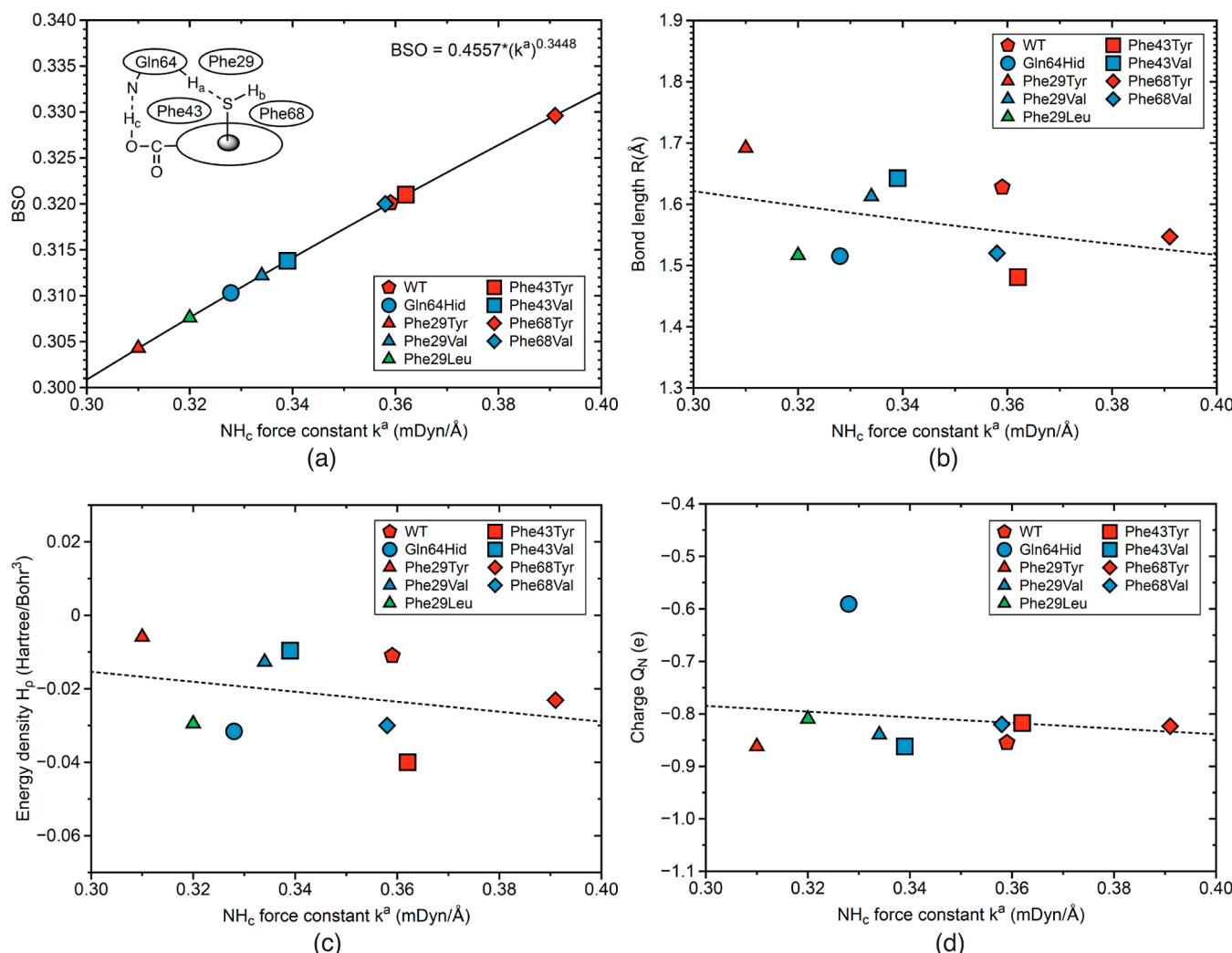


Figure 8. Properties of the NH_c bond. (a) Relationship between local mode force constant k^a and BSO. (b) Relation between local mode force constant k^a and bond length R . (c) Relation between local mode force constant k^a and energy density H_p . (d) Relation between local mode force constant k^a and N atomic charge Q_N . For molecular labels, see the text.

Table 7. Properties of the OH_c Bond: Bond Length R , Local Mode Force Constant k^a , Energy Density at Bond Critical Point H_p , O Atomic Charge Q_O , H Atomic Charge Q_H , Charge Difference ΔQ , and BSO^a

OH_c molecule	R Å	k^a mDyn/Å	H_p Hr/bohr ³	Q_O e	Q_H e	ΔQ e	BSO
WT	1.022	3.629	-0.4748	-0.747	0.515	1.262	0.711
Gln64Hid	1.054	1.972	-0.3914	-0.780	0.521	1.301	0.576
Phe29Tyr	1.010	4.352	-0.5063	-0.734	0.518	1.252	0.757
Phe29Val	1.026	3.252	-0.4639	-0.760	0.516	1.276	0.684
Phe29Leu	1.051	1.982	-0.3953	-0.797	0.513	1.311	0.577
Phe43Tyr	1.010	4.352	-0.5063	-0.734	0.518	1.252	0.757
Phe43Val	1.018	3.798	-0.4838	-0.751	0.519	1.270	0.722
Phe68Tyr	1.042	2.561	-0.4201	-0.779	0.513	1.292	0.630
Phe68Val	1.055	1.973	-0.3909	-0.771	0.511	1.282	0.576

^aFor molecular labels, see the text.

-0.0231 hartree/bohr³) in this series. However, the weakest NH_c bond found for Phe29Tyr ($k^a = 0.310$ mDyn/Å) has the largest bond length ($R = 1.692$ Å) and the least covalent character ($H_p = -0.0059$ hartree/bohr³). According to Figure 8d, there is no correlation between NH_c bond strength and N atomic charge. We also do not observe any trends between the NH_c bond strength for the wild-type protein WT and that of

the protein mutations investigated in this study. The strength of the NH_c bond in WT ($k^a = 0.359$ mDyn/Å) is in the middle of the range for the protein mutations (k^a from 0.310 to 0.391 mDyn/Å). Overall, the strength of the NH_c bond does not correlate with other bond properties, such as the bond length, the energy density, and the N atomic charge. The obvious lack of these correlations can be explained by relatively strong

geometrical constraints involving the molecular fragments forming this bond, such as COO^- , which is chemically bonded to the heme group, and the side chain of the distal residue (Gln64 or His64 δ), which is chemically bonded to the protein backbone. The geometrical constraints involving the SH_a bond after the proton transfer are much less pronounced; therefore, the strength of the SH_a bond correlates better with the other bond properties as presented in the previous sections of this study.

Finally, we investigated the proton acceptor OH_c bond and its connection to the NH_c proton donor bond. As reflected by the data in Table 7 and Figure S3 of the Supporting Information, the OH_c proton acceptor bonds are covalent OH bonds with bond orders in the range of 0.576–0.757. Compared with the O/NH_a proton acceptor bonds discussed above, they are somewhat weaker, resulting from geometrical constraints. Nevertheless, they confirm the double-proton transfer discovered in our work.

CONCLUSIONS

Using the ONIOM QM/MM method, we investigated the interactions between the H_2S ligand coordinated to the iron atom of the heme group of HbI in *Lucina pectinata* for the wild-type protein; three known mutations where distal glutamine is replaced by hydrophobic valine (Gln64Val) and hydrophilic histidine in both protonation forms (Gln64His $_e$, Gln64His $_\delta$); five known mutations of the so-called phenyl cage, replacing the hydrophobic phenylalanines Phe29 and Phe43 with tyrosine (Tyr), valine (Val), or leucine (Leu); and two additional mutations, Phe68Tyr and Phe68Val, complemented by two gas-phase reference models coordinating H_2S and HS^- , in order to complement previous studies with new insights about the binding mechanism at the molecular level. The highlights of this study can be summarized as follows:

1. Wild-type protein and mutations clustered into two distinct groups: Group 1 protein systems with a proton acceptor in the distal protein pocket close to one of the H_2S bonds, and Group 2 protein systems without a hydrogen acceptor close by in the active site of the protein.
2. The interactions between H_2S and HbI of *Lucina pectinata* involve two important elements, namely, binding of H_2S to Fe of the heme group followed by the proton transfer from the HS bond to the distal residue. The distal residue is additionally stabilized by a second proton transfer from the distal residue to COO^- of the propionate group in heme.
3. The FeS bond could be identified as a key player and the strength of the FeS bond depends on two mutual factors, namely, the strength of the HS bond involved in the proton transfer and the electrostatic field of the protein pocket qualifying the FeS bond as a sensitive probe for monitoring changes in H_2S ligation upon protein mutations. These two mutual effects disclose molecular level insights on the affinity of HbI in *Lucina pectinata* binding to H_2S . For mutations where proton transfer is not possible, there is still the influence of the electrostatic field of the protein pocket which modifies the strength of the FeS bond.
4. We could identify the O/NH_a proton acceptor bonds as strong hydrogen bonds and their relation to SH_a proton donor bonds as being complementary, i.e., stronger O/NH_a

NH_a bonds are connected with weaker SH_a bonds and vice versa, confirming that a protein environment can be characterized through FeS bonding as a probe and that the SH_a bond is a good representation of the O/NH_a bonds.

5. The character of the proton acceptor OH_c bond and its connection to the NH_c proton donor bond being involved in the second proton transfer were disclosed. Compared with the O/NH_a proton acceptor bonds, the OH_c bonds are somewhat weaker, resulting from geometrical constraints, and they confirm nevertheless the double-proton transfer mechanism discovered in our work.
6. The FeS bond strength of the investigated molecular systems was assessed via relative BSOs derived from local mode FeS force constants. BSOs are related to local mode force constants via a power relationship based on two references molecules with known BSO and local mode force constant values. We used in this work FeH with a BSO value close to 1 and FeS with a BSO value close to 2. This approach allows us to compare FeS bonds between different protein systems and beyond.

We hope our study will inspire and guide future experimental studies, targeting new promising mutations such as Phe68Tyr and Phe68Val. According to our results, the most interesting protein mutation is Phe43Tyr, which has a relatively large influence on the FeS bond strength. For this protein mutation, we observe an additional hydrogen bond between OH of tyrosine and S, which leads to the formation of an interesting bifurcated hydrogen bond. The Phe68Val mutation also forms a strong FeS bond, and therefore, we expect that the double mutation Phe43Tyr/Phe68Val could lead to an even stronger FeS bond.

ASSOCIATED CONTENT

Supporting Information

The Supporting Information is available free of charge at <https://pubs.acs.org/doi/10.1021/acs.jpca.3c04399>.

Relation between SH_a and SH_b bond lengths and SH_a and FeS bond lengths, properties of O/NH_a bonds, properties of OH_c bonds, relations between selected local force constants k^a , snapshots and sketches of the active proteins sites with selected residues, and snapshots of active site models in the gas phase ([PDF](#))

AUTHOR INFORMATION

Corresponding Author

Elfi Kraka – Computational and Theoretical Chemistry Group (CATCO), Department of Chemistry, Southern Methodist University, Dallas, Texas 75275-0314, United States;
[ORCID: 0000-0002-9658-5626](https://orcid.org/0000-0002-9658-5626); Email: ekraka@smu.edu

Authors

Marek Freindorf – Computational and Theoretical Chemistry Group (CATCO), Department of Chemistry, Southern Methodist University, Dallas, Texas 75275-0314, United States

Juliana Antonio – Computational and Theoretical Chemistry Group (CATCO), Department of Chemistry, Southern Methodist University, Dallas, Texas 75275-0314, United States; [ORCID: 0000-0002-0358-9274](https://orcid.org/0000-0002-0358-9274)

Complete contact information is available at:
<https://pubs.acs.org/10.1021/acs.jpca.3c04399>

Notes

The authors declare no competing financial interest.

ACKNOWLEDGMENTS

This work was supported by the National Science Foundation, Grant CHE 2102461. J.A. thanks the National Science Foundation for a Graduate Research Fellowship Grant DGE-2034834. We thank the Center for Research Computation at SMU for providing generous high-performance computational resources. We thank Alex Lippert for valuable comments.

REFERENCES

- (1) Kamoun, P. Endogenous production of hydrogen sulfide in mammals. *Amino Acids* **2004**, *26*, 243–254.
- (2) Chen, C.-q.; Xin, H.; Zhu, Y.-z. Hydrogen sulfide: third gaseous transmitter, but with great pharmacological potential. *Acta Pharmacol. Sin.* **2007**, *28*, 1709–1716.
- (3) Li, L.; Moore, P. K. Putative biological roles of hydrogen sulfide in health and disease: a breath of not so fresh air? *Trends Pharmacol. Sci.* **2008**, *29*, 84–90.
- (4) Kajimura, M.; Fukuda, R.; Bateman, R. M.; Yamamoto, T.; Suematsu, M. Interactions of Multiple Gas–Transducing Systems: Hallmarks and Uncertainties of CO, NO, and H₂S Gas Biology. *Antioxid. Redox Signaling* **2010**, *13*, 157–192.
- (5) Li, Q.; Lancaster, J. R. Chemical foundations of hydrogen sulfide biology. *Nitric Oxide* **2013**, *35*, 21–34.
- (6) Kimura, H. Signaling Molecules: Hydrogen Sulfide and Polysulfide. *Antioxid. Redox Signaling* **2015**, *22*, 362–376.
- (7) Ono, K.; Akaike, T.; Sawa, T.; Kumagai, Y.; Wink, D. A.; Tantillo, D. J.; Hobbs, A. J.; Nagy, P.; Xian, M.; Lin, J.; et al. Redox chemistry and chemical biology of H₂S, hydrosulfides, and derived species: Implications of their possible biological activity and utility. *Free Radic. Biol. Med.* **2014**, *77*, 82–94.
- (8) Bel托wski, J. Hydrogen sulfide in pharmacology and medicine –An update. *Pharmacol. Rep.* **2015**, *67*, 647–658.
- (9) Szabo, C. A timeline of hydrogen sulfide (H₂S) research: From environmental toxin to biological mediator. *Biochem. Pharmacol.* **2018**, *149*, 5–19.
- (10) Song, Z.; Zhao, L.; Ma, T.; Osama, A.; Shen, T.; He, Y.; Fang, J. Progress and perspective on hydrogen sulfide donors and their biomedical applications. *Med. Res. Rev.* **2022**, *42*, 1930–1977.
- (11) Kelley, J. L.; Arias-Rodriguez, L.; Patacsi Martin, D.; Yee, M.-C.; Bustamante, C. D.; Tobler, M. Mechanisms Underlying Adaptation to Life in Hydrogen Sulfide–Rich Environments. *Mol. Biol. Evol.* **2016**, *33*, 1419–1434.
- (12) Olson, K. R.; Straub, K. D. The Role of Hydrogen Sulfide in Evolution and the Evolution of Hydrogen Sulfide in Metabolism and Signaling. *Physiology* **2016**, *31*, 60–72.
- (13) Olson, K. R. Hydrogen sulfide, reactive sulfur species and coping with reactive oxygen species. *Free Radic. Biol. Med.* **2019**, *140*, 74–83.
- (14) Zhu, J.; Ligi, S.; Yang, G. An evolutionary perspective on the interplays between hydrogen sulfide and oxygen in cellular functions. *Arch. Biochem. Biophys.* **2021**, *707*, 108920.
- (15) Rizzi, M.; Wittenberg, J. B.; Coda, A.; Ascenzi, P.; Bolognesi, M. Structural Bases for Sulfide Recognition in *Lucina pectinata* Hemoglobin I. *J. Mol. Biol.* **1996**, *258*, 1–5.
- (16) Kraus, D. W.; Wittenberg, J. B. Hemoglobins of the *Lucina pectinata*/bacteria symbiosis. I. Molecular properties, kinetics and equilibria of reactions with ligands. *J. Biol. Chem.* **1990**, *265*, 16043–16053.
- (17) Pietri, R.; Lewis, A.; León, R. G.; Casabona, G.; Kiger, L.; Yeh, S.-R.; Fernandez-Alberti, S.; Marden, M. C.; Cadilla, C. L.; López-Garriga, J. Factors Controlling the Reactivity of Hydrogen Sulfide with Hemeproteins. *Biochemistry* **2009**, *48*, 4881–4894.
- (18) Pietri, R.; Román-Morales, E.; López-Garriga, J. Hydrogen Sulfide and Hemeproteins: Knowledge and Mysteries. *Antioxid. Redox Signaling* **2011**, *15*, 393–404.
- (19) Vitvitsky, V.; Yadav, P. K.; Kurthen, A.; Banerjee, R. Sulfide Oxidation by a Noncanonical Pathway in Red Blood Cells Generates Thiosulfate and Polysulfides. *J. Biol. Chem.* **2015**, *290*, 8310–8320.
- (20) Bostelaar, T.; Vitvitsky, V.; Kumutima, J.; Lewis, B. E.; Yadav, P. K.; Brunold, T. C.; Filipovic, M.; Lehner, N.; Stemmler, T. L.; Banerjee, R. Hydrogen Sulfide Oxidation by Myoglobin. *J. Am. Chem. Soc.* **2016**, *138*, 8476–8488.
- (21) Boubeta, F. M.; Bari, S. E.; Estrin, D. A.; Boechi, L. Access and Binding of H₂S to Hemeproteins: The Case of HbI of *Lucina pectinata*. *J. Phys. Chem. B* **2016**, *120*, 9642–9653.
- (22) Vitvitsky, V.; Yadav, P. K.; An, S.; Seravalli, J.; Cho, U.-S.; Banerjee, R. Structural and Mechanistic Insights into Hemoglobin-catalyzed Hydrogen Sulfide Oxidation and the Fate of Polysulfide Products. *J. Biol. Chem.* **2017**, *292*, 5584–5592.
- (23) Jensen, B.; Fago, A. Reactions of ferric hemoglobin and myoglobin with hydrogen sulfide under physiological conditions. *J. Inorg. Biochem.* **2018**, *182*, 133–140.
- (24) Boubeta, F. M.; Bieza, S. A.; Bringas, M.; Palermo, J. C.; Boechi, L.; Estrin, D. A.; Bari, S. E. Hemeproteins as Targets for Sulfide Species. *Antioxid. Redox Signaling* **2020**, *32*, 247–257.
- (25) Pluth, M. D.; Tonsetich, Z. J. Hydrosulfide complexes of the transition elements: diverse roles in bioinorganic, cluster, coordination, and organometallic chemistry. *Chem. Soc. Rev.* **2020**, *49*, 4070–4134.
- (26) Weber, R. E.; Vinogradov, S. N. Nonvertebrate Hemoglobins: Functions and Molecular Adaptations. *Physiol. Rev.* **2001**, *81*, 569–628.
- (27) Bailly, X.; Vinogradov, S. The sulfide binding function of annelid hemoglobins: relic of an old biosystem? *J. Inorg. Biochem.* **2005**, *99*, 142–150.
- (28) Kraus, D. W.; Wittenberg, J. B.; Lu, J. F.; Peisach, J. Hemoglobins of the *Lucina pectinata*/bacteria symbiosis. II. An electron paramagnetic resonance and optical spectral study of the ferric proteins. *J. Biol. Chem.* **1990**, *265*, 16054–16059.
- (29) Dulac, M.; Melet, A.; Galardon, E. Reversible Detection and Quantification of Hydrogen Sulfide by Fluorescence Using the Hemoglobin I from *Lucina pectinata*. *ACS Sens.* **2018**, *3*, 2138–2144.
- (30) Ramos-Alvarez, C.; Yoo, B.-K.; Pietri, R.; Lamarre, L.; Martin, J.-L.; Lopez-Garriga, J.; Negrier, M. Reactivity and Dynamics of H₂S, NO, and O₂ Interacting with Hemoglobins from *Lucina pectinata*. *Biochemistry* **2013**, *52*, 7007–7021.
- (31) Montes-Rodríguez, I. M.; Cadilla, C. L.; López-Garriga, J.; González-Méndez, R. Bioinformatic Characterization and Molecular Evolution of the *Lucina pectinata* Hemoglobins. *Genes* **2022**, *13*, 2041.
- (32) Pietri, R.; León, R. G.; Kiger, L.; Marden, M. C.; Granell, L. B.; Cadilla, C. L.; López-Garriga, J. Hemoglobin I from *Lucina pectinata*: A model for distal heme-ligand control. *Biochim. Biophys. Acta, Proteins Proteomics* **2006**, *1764*, 758–765.
- (33) Kraka, E.; Quintano, M.; La Force, H. W.; Antonio, J. J.; Freindorf, M. The Local Vibrational Mode Theory and Its Place in the Vibrational Spectroscopy Arena. *J. Phys. Chem. A* **2022**, *126*, 8781–8798.
- (34) Kraka, E.; Zou, W.; Tao, Y. Decoding Chemical Information from Vibrational Spectroscopy Data: Local Vibrational Mode Theory. *WIREs: Comput. Mol. Sci.* **2020**, *10*, 1480.
- (35) Bader, R. F. W. A quantum theory of molecular structure and its applications. *Chem. Rev.* **1991**, *91*, 893–928.
- (36) Bader, R. F. W. *Atoms in Molecules: A Quantum Theory (International Series of Monographs on Chemistry)*; Clarendon Press, 1994.
- (37) Bader, R. F. W. The Quantum Mechanical Basis of Conceptual Chemistry. *Monatshefte für Chemie* **2005**, *136*, 819–854.

- (38) Reed, A. E.; Curtiss, L. A.; Weinhold, F. Intermolecular Interactions from a Natural Bond Orbital, Donor-Acceptor Viewpoint. *Chem. Rev.* **1988**, *88*, 899–926.
- (39) Warshel, A.; Karplus, M. Calculation of ground and excited state potential surfaces of conjugated molecules. I. Formulation and parametrization. *J. Am. Chem. Soc.* **1972**, *94*, 5612–5625.
- (40) Warshel, A.; Levitt, M. Theoretical studies of enzymic reactions: Dielectric, electrostatic and steric stabilization of the carbonium ion in the reaction of lysozyme. *J. Mol. Biol.* **1976**, *103*, 227–249.
- (41) van der Kamp, M. W.; Mulholland, A. J. Combined Quantum Mechanics/Molecular Mechanics (QM/MM) Methods in Computational Enzymology. *Biochemistry* **2013**, *52*, 2708–2728.
- (42) Tzeliou, C. E.; Mermigki, M. A.; Tzeli, D. Review on the QM/MM Methodologies and Their Application to Metalloproteins. *Molecules* **2022**, *27*, 2660.
- (43) Hratchian, H. P.; Parandekar, P. V.; Raghavachari, K.; Frisch, M. J.; Vreven, T. QM:QM electronic embedding using Mulliken atomic charges: Energies and analytic gradients in an ONIOM framework. *J. Chem. Phys.* **2008**, *128*, 034107.
- (44) Mayhall, N. J.; Raghavachari, K.; Hratchian, H. P. ONIOM-based QM:QM electronic embedding method using Lowdin atomic charges: Energies and analytic gradients. *J. Chem. Phys.* **2010**, *132*, 114107.
- (45) Hratchian, H. P.; Kruckau, A. V.; Parandekar, P. V.; Frisch, M. J.; Raghavachari, K. QM:QM embedding using electronic densities within an ONIOM framework: Energies and analytic gradients. *J. Chem. Phys.* **2011**, *135*, 014105.
- (46) Mayhall, N. J.; Raghavachari, K. Molecules-in-Molecules: An Extrapolated Fragment-Based Approach for Accurate Calculations on Large Molecules and Materials. *J. Chem. Theory Comput.* **2011**, *7*, 1336–1343.
- (47) Thapa, B.; Beckett, D.; Erickson, J.; Raghavachari, K. Theoretical Study of Protein–Ligand Interactions Using the Molecules-in-Molecules Fragmentation-Based Method. *J. Chem. Theory Comput.* **2018**, *14*, 5143–5155.
- (48) Thapa, B.; Beckett, D.; Jovan Jose, K. V.; Raghavachari, K. Assessment of Fragmentation Strategies for Large Proteins Using the Multilayer Molecules-in-Molecules Approach. *J. Chem. Theory Comput.* **2018**, *14*, 1383–1394.
- (49) Thapa, B.; Raghavachari, K. Energy Decomposition Analysis of Protein–Ligand Interactions Using Molecules-in-Molecules Fragmentation-Based Method. *J. Chem. Inf. Model.* **2019**, *59*, 3474–3484.
- (50) Thapa, B.; Erickson, J.; Raghavachari, K. Quantum Mechanical Investigation of Three-Dimensional Activity Cliffs Using the Molecules-in-Molecules Fragmentation-Based Method. *J. Chem. Inf. Model.* **2020**, *60*, 2924–2938.
- (51) Tripathy, V.; Mayhall, N. J.; Raghavachari, K. ONIOM Method with Charge Transfer Corrections (ONIOM-CT): Analytic Gradients and Benchmarking. *J. Chem. Theory Comput.* **2022**, *18*, 6052–6064.
- (52) Barone, V.; Alessandrini, S.; Biczysko, M.; Cheeseman, J. R.; Clary, D. C.; McCoy, A. B.; DiRisio, R. J.; Neese, F.; Melosso, M.; Puzzarini, C. Computational molecular spectroscopy. *Nat. Rev. Methods Primers* **2021**, *1*, 38.
- (53) Kelley, J. D.; Leventhal, J. J. *Problems in Classical and Quantum Mechanics: Normal Modes and Coordinates*; Springer, 2017; pp 95–117.
- (54) Califano, S. *Vibrational States*; Wiley: London, 1976.
- (55) Wilson, E. B.; Decius, J. C.; Cross, P. C. M. *Molecular Vibrations. The Theory of Infrared and Raman Vibrational Spectra*; McGraw-Hill: New York, 1955; pp 59–136.
- (56) Wilson, E. B. Some Mathematical Methods for the Study of Molecular Vibrations. *J. Chem. Phys.* **1941**, *9*, 76–84.
- (57) Konkoli, Z.; Cremer, D. A New Way of Analyzing Vibrational Spectra. I. Derivation of Adiabatic Internal Modes. *Int. J. Quantum Chem.* **1998**, *67*, 1–9.
- (58) Konkoli, Z.; Larsson, J. A.; Cremer, D. A New Way of Analyzing Vibrational Spectra. II. Comparison of Internal Mode Frequencies. *Int. J. Quantum Chem.* **1998**, *67*, 11–27.
- (59) Cremer, D.; Kraka, E. From Molecular Vibrations to Bonding, Chemical Reactions, and Reaction Mechanism. *Curr. Org. Chem.* **2010**, *14*, 1524–1560.
- (60) Kraka, E.; Larsson, J. A.; Cremer, D. In *Computational Spectroscopy*; Grunenberg, J., Ed.; Wiley: New York, 2010; pp 105–149.
- (61) Mayer, I. Charge, bond order and valence in the ab initio SCF theory. *Chem. Phys. Lett.* **1983**, *97*, 270–274.
- (62) Mayer, I. Bond orders and valences from ab initio wave functions. *Int. J. Quantum Chem.* **1986**, *29*, 477–483.
- (63) Mayer, I. Bond order and valence indices: A personal account. *J. Comput. Chem.* **2007**, *28*, 204–221.
- (64) Cremer, D.; Kraka, E. Chemical Bonds without Bonding Electron Density? Does the Difference Electron-Density Analysis Suffice for a Description of the Chemical Bond? *Angew. Chem., Int. Ed.* **1984**, *23*, 627–628.
- (65) Cremer, D.; Kraka, E. A Description of the Chemical Bond in Terms of Local Properties of Electron Density and Energy. *Croat. Chem. Acta* **1984**, *57*, 1259–1281.
- (66) Kraka, E.; Cremer, D. Theoretical Models of Chemical Bonding. In *The Concept of the Chemical Bond*; Maksic, Z. B., Ed.; Springer Verlag: Heidelberg, 1990; Vol. 2, pp 453–542.
- (67) Chung, L. W.; Sameera, W. M. C.; Ramozzi, R.; Page, A. J.; Hatanaka, M.; Petrova, G. P.; Harris, T. V.; Li, X.; Ke, Z.; Liu, F.; et al. The ONIOM Method and Its Applications. *Chem. Rev.* **2015**, *115*, 5678–5796.
- (68) Pettersen, E. F.; Goddard, T. D.; Huang, C. C.; Couch, G. S.; Greenblatt, D. M.; Meng, E. C.; Ferrin, T. E. UCSF Chimera—A visualization system for exploratory research and analysis. *J. Comput. Chem.* **2004**, *25*, 1605–1612.
- (69) Case, D. A.; Ben-Shalom, I. Y.; Brozell, S. R.; Cerutti, D. S.; Cheatham, T. E.; Cruzeiro, V. W. D.; Darden, T. A.; Duke, R. E.; Ghoreishi, D.; Gilson, M. K.; et al. AMBER; University of California: San Francisco, 2018.
- (70) Jorgensen, W. L.; Chandrasekhar, J.; Madura, J. D.; Impey, R. W.; Klein, M. L. Comparison of simple potential functions for simulating liquid water. *J. Chem. Phys.* **1983**, *79*, 926–935.
- (71) Ernzerhof, M.; Perdew, J. P. Generalized gradient approximation to the angle- and system-averaged exchange hole. *J. Chem. Phys.* **1998**, *109*, 3313–3320.
- (72) Perdew, J. P.; Burke, K.; Ernzerhof, M. Generalized Gradient Approximation Made Simple. *Phys. Rev. Lett.* **1996**, *77*, 3865–3868.
- (73) Ditchfield, R.; Hehre, W. J.; Pople, J. A. Self-Consistent Molecular–Orbital Methods. IX. An Extended Gaussian–Type Basis for Molecular–Orbital Studies of Organic Molecules. *J. Chem. Phys.* **1971**, *54*, 724–728.
- (74) Adamo, C.; Barone, V. Toward Reliable Density Functional Methods without Adjustable Parameters: The PBE0 Model. *J. Chem. Phys.* **1999**, *110*, 6158–6170.
- (75) Zhao, S.; Li, Z.-H.; Wang, W.-N.; Liu, Z.-P.; Fan, K.-N.; Xie, Y.; Schaefer, H. F. Is the uniform electron gas limit important for small Ag clusters? Assessment of different density functionals for Ag_n (n<4). *J. Chem. Phys.* **2006**, *124*, 184102.
- (76) Cramer, C. J.; Truhlar, D. G. Density functional theory for transition metals and transition metal chemistry. *Phys. Chem. Chem. Phys.* **2009**, *11*, 10757–10816.
- (77) Li, S.; Hennigan, J. M.; Dixon, D. A.; Peterson, K. A. Accurate Thermochemistry for Transition Metal Oxide Clusters. *J. Phys. Chem. A* **2009**, *113*, 7861–7877.
- (78) Safo, M. K.; Gupta, G. P.; Walker, F. A.; Scheidt, W. R. Models of the cytochromes b. Control of axial ligand orientation with a hindered porphyrin system. *J. Am. Chem. Soc.* **1991**, *113*, 5497–5510.
- (79) Frisch, M. J.; Trucks, G. W.; Schlegel, H. B.; Scuseria, G. E.; Robb, M. A.; Cheeseman, J. R.; Scalmani, G.; Barone, V.; Petersson, G. A.; Nakatsuji, H.; et al. *Gaussian 16*; Gaussian Inc.: Wallingford CT, 2016.
- (80) Zou, W.; Tao, Y.; Freindorf, M.; Makoś, M. Z.; Verma, N.; Cremer, D.; Kraka, E. Local Vibrational Mode Analysis (LModeA).

Computational and Theoretical Chemistry Group (CATCO); Southern Methodist University: Dallas, TX, USA, 2023.

(81) Glendening, E. D.; Badenhoop, J. K.; Reed, A. E.; Carpenter, J. E.; Bohmann, J. A.; Morales, C. M.; Landis, C. R.; Weinhold, F. NBO6; Theoretical Chemistry Institute, University of Wisconsin: Madison, 2013.

(82) Keith, T. A. AIMALL. TK Gristmill Software; Overland Park KS, 2017.

(83) Freindorf, M.; Kraka, E. Critical Assessment of the FeC and CO Bond strength in Carboxymyoglobin - A QM/MM Local Vibrational Mode Study. *J. Mol. Model.* **2020**, *26*, 281.

(84) Freindorf, M.; Delgado, A. A. A.; Kraka, E. CO bonding in hexa- and pentacoordinate carboxy-neuroglobin: A quantum mechanics/molecular mechanics and local vibrational mode study. *J. Comput. Chem.* **2022**, *43*, 1725–1746.

(85) Badger, R. M. A Relation between Internuclear Distances and Bond Force Constants. *J. Chem. Phys.* **1934**, *2*, 128–131.

CAS BIOFINDER DISCOVERY PLATFORM™

ELIMINATE DATA SILOS. FIND WHAT YOU NEED, WHEN YOU NEED IT.

A single platform for relevant, high-quality biological and toxicology research

Streamline your R&D

CAS
A division of the
American Chemical Society